ELSEVIER

Solar Energy Materials & Solar Cells 65 (2001) 63–69

Solar Energy Materials & Solar Cells

www.elsevier.com/locate/solmat

Numerical simulation of electron-beam-induced current near a silicon grain boundary and impact of a p–n junction space charge region

Richard Corkish[a,*], Pietro P. Altermatt[a], Gernot Heiser[a,b]

[a]*Photovoltaics Special Research Centre, University of New South Wales, Sydney 2052, Australia*
[b]*School of Computer Science and Engineering, University of New South Wales, Sydney 2052, Australia*

Abstract

Three-dimensional numerical simulations of electron-beam-induced current (EBIC) near a vertical silicon grain boundary are demonstrated. They are compared with an analytical model which excludes the effect of carrier generation other than in the bulk base region of a solar cell structure. We demonstrate that in a wide range of solar cell structures recombination in the space charge region (SCR) significantly affects the EBIC results and hence needs to be included in the data evaluation. Apart from these findings, simulations of a realistic silicon solar cell structure (thick emitter, field-dependent mobility, etc.) are demonstrated.

Keywords: EBIC; Grain boundary; Numerical simulation; Silicon

1. Introduction

Electron-beam-induced current (EBIC) is a useful technique for the investigation of point and extended defects in semiconductors. However, comprehensive physical models are needed for the extraction of quantitative information since EBIC data are influenced by a wide range of physical phenomena. Some of these difficulties can be alleviated by the use of numerical simulation for direct comparison with experimental results. In this work we demonstrate the 3D numerical simulation of current collection in silicon by a horizontal p–n junction as a response to illumination by a vertical

* Corresponding author.
E-mail address: r.corksih@unsw.edu.au (R. Corkish).

0927-0248/01/$ - see front matter
PII: S0927-0248(00)00078-7

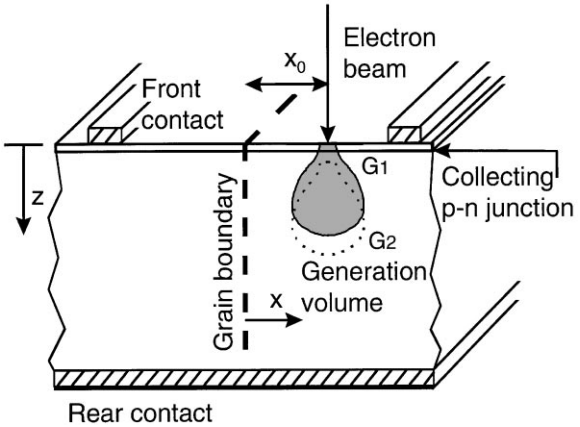

Fig. 1. Schematic representation of electron beam current method for grain-boundary analysis considered in this work. Two positions are shown for the generation volume. The normal, G1, position extends downwards from the silicon surface. The dashed, G2, position is an artificial case in which the generation volume extends downwards from the lower edge of the space charge region.

electron beam (Fig. 1) in the vicinity of a vertical grain boundary. Previously, Stemmer [1] used (Monte Carlo) MC methods to simulate LBIC near grain boundaries that were modelled as regions of finite thickness with reduced minority-carrier lifetime. Tabet and Ledra [2], adopted a similar grain-boundary model and calculated the EBIC by MC methods using both point-source and 3D MC models for the generation.

The model by Donolato [3] provides analytical expressions for the EBIC near a vertical grain boundary between homogeneous grains of identical diffusion length. The emitter and space charge regions (SCR) are neglected entirely while the base is assumed to be of infinite thickness and the grain boundary may be described as a simple planar interface with a constant recombination velocity. We compare our numerical simulation model for grain-boundary EBIC with Donolato's analytical model under an appropriate set of assumptions. Our approach differs from others [1,2] in the model used to describe the grain boundary and in the use of a general-purpose classical simulator rather than MC modelling. The error that arises from the neglect in the analytical model of generation in the SCR is demonstrated by fitting the analytical expression to simulated grain-boundary EBIC profiles which either include or exclude SCR generation. A more realistic solar cell structure is also simulated.

2. Comparison between numerical simulations and analytical model

The three-dimensional numerical EBIC model used for this work is an extension of a prior two-dimensional model [4]. It is implemented in the DESSIS [5] semiconductor device simulator which uses the "box" or "finite volumes" method for discretisation of the device volume to solve the coupled set of Poisson, electron and hole

continuity, and drift-diffusion differential equations. An empirically based model [6] was used to describe the carrier generation rate. The mesh has been optimised for a narrow (beam diameter = 10 nm) beam of 30 keV electrons. Around 3×10^5 mesh points were necessary to ensure that simulated currents were precise within $\pm 0.5\%$. The emitter was modelled as a Gaussian diffusion with donor density of $10^{19}\,\mathrm{cm}^{-3}$ at the surface and the junction occurring 10 nm below the surface. This very shallow emitter was used to approximate the conditions for the analytical model. In order to ensure an identical diffusion length throughout the structure, Auger recombination and bandgap narrowing were excluded from the simulations and the carrier mobilities were made independent of doping. Zero surface recombination velocity is assumed at the top and bottom surfaces. The simulation region was of sufficient depth to ensure that the results were independent of device thickness. Results presented in the next section were produced using a more "realistic" device model.

EBIC contrast, c, is defined by

$$c = 1 - I(x_0)/I_0, \tag{1}$$

where $I(x_0)$ is the collected EBIC when the beam is a distance, x_0, from the grain boundary and I_0 is the background EBIC, the asymptote for $I(x_0)$ as $x_0 \to \infty$.

Simulations were carried out for an isolated vertical grain boundary between two identical silicon grains with diffusion length (L) equal to 5.48 μm, which is less than the maximum depth at which generation occurs (7.3 μm) [6]. The integrated generation rate due to the beam was set at $10^{11}\,\mathrm{s}^{-1}$, ensuring low-injection conditions. Fig. 2(a) compares I_0 and $I(x_0)$ results from the analytical model with simulated results for base doping levels of $N_A = 10^{16}$ and $10^{18}\,\mathrm{cm}^{-3}$. Note the large separation of the simulated results for both I_0 and $I(x_0)$ with $10^{16}\,\mathrm{cm}^{-3}$ base doping from the corresponding analytical results. The analytical results are seen to agree much more closely with the simulated values for $10^{18}\,\mathrm{cm}^{-3}$ base doping. The corresponding contrast curves are shown in Fig. 2(b). For the more lightly doped base there is a significant contrast difference between the simulated values and the analytical curve while the simulations for the more heavily doped base agree with the analytical model. Since the diffusion length is identical in each case, the differences must be due to the inclusion in the simulations of a SCR (having different thicknesses depending on the base doping) and its exclusion in the analytical treatment. That explanation is confirmed by simulation of the artificial situation in which the electron beam is assumed to pass through the emitter and SCR without interacting with the silicon (G2 position of the generation volume in Fig. 1). Then the analytical and simulated results are in close agreement (Fig. 2b) for both doping densities. The (G2 position) contrast was also simulated for two other v_s values and the results agree closely with analytical calculations (Fig. 3).

Further simulations were carried out with longer diffusion lengths, assuming a base doping level of $10^{16}\,\mathrm{cm}^{-3}$ in each case. The results for the background currents for generation from the surface and from the lower SCR were compared with an analytical expression for background current [6],

$$I_0 = \frac{qg_0}{R}\left[\int_0^{1.1R} \exp(-z/L)\Lambda(z)\right]\mathrm{d}z, \tag{2}$$

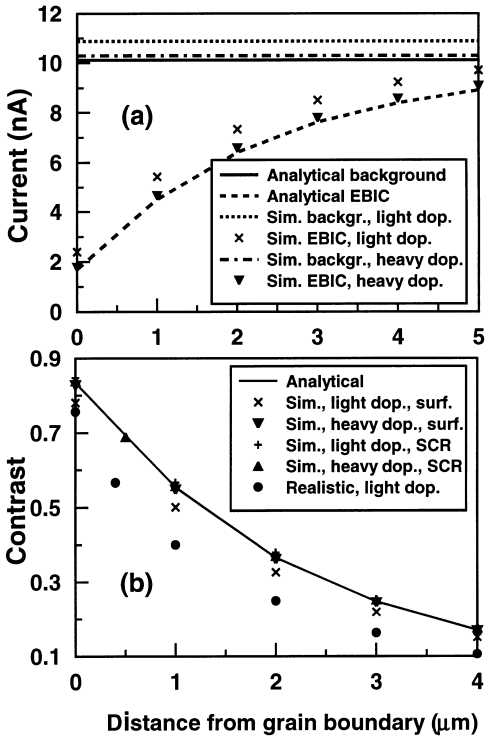

Fig. 2. (a) Horizontal lines show EBIC background currents from an analytical model and from simulations with light ($10^{16}\,cm^{-3}$) and heavy ($10^{18}\,cm^{-3}$) base doping levels where the carrier mobility is the same in each case. The curved line and sets of points are the corresponding EBIC responses near a grain boundary with $v_s = 10^7\,cm\,s^{-1}$. The generation volume extended from the device surface for each case (G1 position). (b) contrast curves calculated from the currents in (a) are labelled "G1" in the legend. Also shown in (b) and labelled "G2" in the legend, are simulated contrast points for the same doping levels with the top of the generation aligned with the lower edge of the space-charge region. The results of simulation of a "realistic" structure are included.

which neglects generation in the SCR, and with a modified form which assumes unity collection efficiency for carriers generated in the SCR (SCR recombination is included in all the numerical modelling and is neglected only in this expression):

$$I_0 = \frac{qg_0}{R}\left\{\int_0^{z_{SCR}} \Lambda(z)\,dz + \int_{z_{SCR}}^{1.1R} \exp[(z_{SCR} - z)/L]\Lambda(z)\right\}dz, \tag{3}$$

where q is the electron charge, g_0 is the integrated generation rate of carrier pairs, R is the electron penetration range, z is the depth below the surface, Λ is the laterally integrated depth dose, and z_{SCR} is the depth of the lower edge of the SCR [6]. The simulated background current agreed with Eq. (2) for the G1 position and with Eq. (3) for the G2 position.

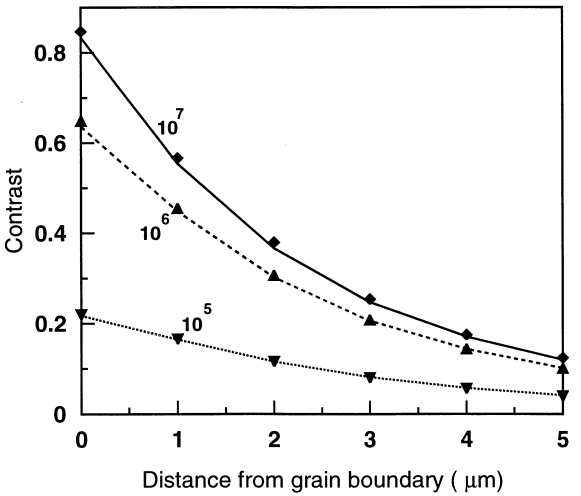

Fig. 3. Comparison of analytical (lines) and simulation (points) methods of calculating grain-boundary contrast for three values of v_s: 10^5, 10^6, and 10^7 cm s^{-1}. The base doping is set to 10^{16} cm^{-3}, $L = 5.48$ μm, electron mobility = 1160 cm^2 V^{-1} s^{-1} and the generation volume extends downwards from the lower SCR edge at 0.4 μm below the surface.

3. Numerical simulation of realistic device structures

A simulated contrast profile was produced using a more realistic solar cell model for comparison with the results from the less practical devices considered above. The results are included as a set of points in Fig. 2(b) for minority carrier lifetime parameter of 10 ns (as in the $L = 5.48$ μm cases considered above) and base doping of 10^{16} cm^{-3}. The changes made to the model were: thicker (1 μm) emitter; front oxide layer; front surface recombination velocities of 4×10^3 cm s^{-1}; bandgap narrowing for heavy doping; mobility variation with carrier concentration; velocity saturation at high field intensities; variable surface charges at the grain-boundary; and Auger recombination.

4. Parameter extraction

Contrast curves were simulated for $L = 5.48$ μm and $v_s = 10^7$ cm s^{-1} with light (10^{16} cm^{-3}) and heavy (10^{18} cm^{-3}) base doping for each position of the generation volume and analytical curves were fitted [7] (Fig. 4). For a lightly doped base, generation in the SCR leads to significant error when the analytical expression is fitted to the simulated results. The error, and especially that in the fitted L value, is reduced when the SCR generation is minimised. Extraction of parameters from a realistically simulated contrast profile yielded an L value in error by 48% (Fig. 4). This is at least

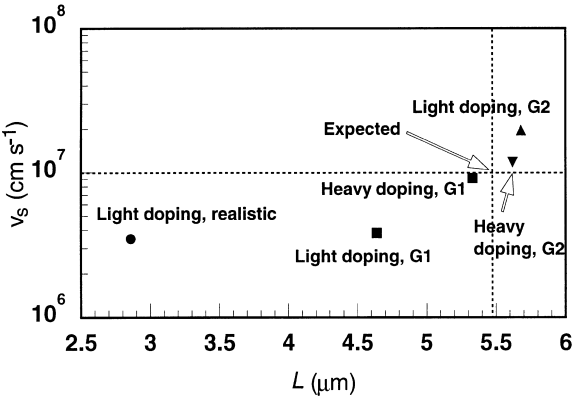

Fig. 4. Values of L and v_s extracted from simulated contrast curves by fitting Donolato's analytical expression.

partly due to the fact that the minority carrier mobility is no longer spatially constant due to velocity saturation in the electric field across the grain boundary.

5. Conclusions

We have demonstrated a 3D numerical simulation model for grain-boundary EBIC response problems and compared it with an established analytical model under the same simplifying restrictions. We have shown that the analytical model leads to highly inaccurate results under certain realistic conditions and have established the conditions under which it produces reasonable results. This numerical model will allow the detailed investigation of complicated arrangements of grain boundaries for which analytical treatments are impractical and allows the inclusion of more sophisticated physical models. Furthermore, since the simulator is able to treat arbitrary injection conditions, the extraction of material parameters from experimental profiles does not require the experiments to be carried out under low injection conditions.

Acknowledgements

The Photovoltaics Special Research Centre was supported by the Australian Research Council's (ARC) Special Research Centres Scheme and by Pacific Power. G.H. and R.C. acknowledge the financial support of an ARC Large Grant and Small Grant. P.P.A. acknowledges the financial support of an ARC Postdoctoral Fellowship. R.C. is grateful to Dr. Armin Aberle, Dr. Mark Keevers, and Mr. Jürgen Schumacher (ISE, Freiburg) for helpful discussions.

References

[1] M. Stemmer, Monte Carlo simulation of the minority-carrier recombination at and around grain boundaries surrounded by a denuded zone revealed by light-beam-induced current mapping, Mater. Sci. Eng. B 24 (1994) 180.
[2] N. Tabet, M. Ledra, Monte Carlo simulation of the EBIC grain boundary contrast in semiconductors, Mater. Sci. Eng. B 42 (1996) 181.
[3] C. Donolato, Theory of beam induced current characterization of grain boundaries in polycrystalline solar cells, J. Appl. Phys. 54 (1983) 1314.
[4] S.A. Edmiston, G. Heiser, A.B. Sproul, M.A. Green, Improved modelling of grain-boundary recombination in bulk and p–n junction regions of polycrystalline silicon solar cells, J. Appl. Phys. 80 (1996) 6783.
[5] Integrated systems engineering AG, DESSIS-ISE Manual. Release 4.0 (1997).
[6] C. Donolato, An analytical model of SEM and STEM charge collection images of dislocations in thin semiconductor layers. I. Minority carrier generation, diffusion, and collection, Phys. Stat. Sol. A 65 (1981) 649.
[7] R. Corkish, T. Puzzer, A.B. Sproul, K.L. Luke, Quantitative interpretation of electron-beam-induced current grain boundary contrast profiles with application to silicon, J. Appl. Phys. 84 (1998) 5473.